Ionization Energies and Bonding Scheme of Multiple-Decker Sandwich Clusters: M_n (C6H6)_n+1

ARTICLE *in* THE JOURNAL OF PHYSICAL CHEMISTRY A · APRIL 1999

Impact Factor: 2.69 · DOI: 10.1021/jp990093a

2 AUTHORS:

Tomokazu Yasuike
The Open University of Japan
25 PUBLICATIONS **369** CITATIONS
SEE PROFILE

Satoshi Yabushita
Keio University
80 PUBLICATIONS **2,380** CITATIONS
SEE PROFILE

Ionization Energies and Bonding Scheme of Multiple-Decker Sandwich Clusters: $M_n(C_6H_6)_{n+1}$

Tomokazu Yasuike and Satoshi Yabushita*

Department of Chemistry, Faculty of Science and Technology, Keio University, 3-14-1 Hiyoshi, Kohoku-ku, Yokohama 223-8522, Japan

Received: January 7, 1999; In Final Form: April 9, 1999

The preparation of multiple-decker sandwich clusters $V_n(C_6H_6)_{n+1}$ and their large size dependence of the ionization energies have recently been reported by Kaya and his co-workers (*J. Phys. Chem*. **1995**, *99*, 3053). In the present paper, the bonding scheme between benzene and metal atoms (Ti, V, and Cr) was investigated by using Mayer's bond order analysis with ab initio MO calculations, and it was attributed mainly to the delocalization of metal dδ electrons via the LUMOs of the benzene molecules. Moreover, the lowest ionization of most multiple-decker sandwich clusters was found to occur from the upper end of the dδ orbitals, and the large size dependence of the ionization energies was also related to the significant one-dimensional delocalization of these dδ electrons. The proposed Hückel type treatment for these frontier orbitals explains the above properties very simply and suggests also the large size dependence of the photoabsorption band positions and even the thermodynamical stability of the one-dimensional polymer materials denoted by $[M(C_6H_6)]_\infty$. Besides, the ionization energies of these polymeric species are estimated to be 2.68, 3.15, and 4.28 eV for M = Ti, V, and Cr, respectively.

1. Introduction

In the last two decades, some physical chemists have applied molecular beam technique to organometallic compounds and have opened up "gas-phase organometallic chemistry".[1] This movement has proven to be very important to reduce empirical aspects in the conventional organometallic chemistry. In fact, many novel compounds have been synthesized by applying the cluster formation methods such as a modified laser vaporization method.[2−5]

Under this situation, Kaya and his co-workers have reported the preparation of multiple-decker sandwich clusters, in which benzene and vanadium are considered to lie heaped up alternatively.[2] The preparation of such clusters is very interesting because they have an ideal one-dimensional structure to have charge-density-wave (CDW) or spin-density-wave (SDW) states. Particular attention has recently been paid to the CDW conductors because of the strikingly nonlinear and anisotropic electrical properties, gigantic dielectric constants, unusual elastic properties, and rich dynamical behavior.[6] Though multiple-decker sandwich clusters have been the most probable candidate for such one-dimensional materials,[7] nobody has ever succeeded in their preparation. A related compound $[Ni(C_3B_2(CH_3)_4H)]_\infty$ has been actually characterized as a microcrystalline material with a remarkably high electrical conductivity of 0.2 $(\Omega\ cm)^{-1}$.[8] This value exceeds even that for undoped polyacetylene considerably, and such organometallic sandwich polymers are considered to form a new class of one-dimensional conductors.

Kaya and his co-workers have also reported the following two observations for multiple-decker sandwich clusters. First, when the V atom is changed to Ti or Cr, the formation of such clusters becomes unfavorable. Second, the ionization energies of the clusters decrease drastically with increasing the cluster size. We have theoretically explained the former in a previous paper.[9] In the present paper, we elucidate the latter, and investigate also the bonding characters and magnetic properties based on ab initio methods. In addition, the difference in the bonding characters between these clusters and ferrocene, which is another typical sandwich complex, is examined.

In section 2, we describe some computational details. We give the results and discussion for $M(C_6H_6)_2$ in sections 3.1 to 3.3 and those for multiple-decker sandwich clusters in 3.4 to 3.8. Conclusions are given in section 4.

2. Computational Details

The main subject of the present paper is to understand properties of the large size complexes of $M_n(C_6H_6)_m$ systematically, and we chose the MIDI basis set[10] built in the GAMESS program[11] with a compromise between its accuracy and computational economy.

We have estimated the vertical ionization energies by three different methods: (1) Koopmans' theorem (at the optimized geometry with the RHF/ROHF methods); (2) ΔMP2 (at the optimized geometry with the RHF/ROHF methods); (3) ΔDFT (at the optimized geometry with the DFT method). In the DFT calculations, the B3LYP functional[12] was adopted. Moreover, most geometry optimizations were carried out within D_{6h} symmetry, since the energy changes due to symmetry lowering in several examples were always negligibly small, as shown later.

In the application of Koopmans' theorem to open shell $V_n(C_6H_6)_{n+1}$ with the ROHF method, we must pay a special attention to the form of the diagonal block of the Fock operators and used the following forms to define the orbital energies for closed- and open-shell orbitals, respectively:

* E-mail: yabusita@chem.keio.ac.jp. Fax: +81-45-563-5967.

10.1021/jp990093a CCC: $18.00
Published on Web 05/20/1999

$$F^{\text{closed}} = h + \sum_{i}^{\text{closed}} (2J_i - K_i) + \sum_{i}^{\text{open}} J_i$$

$$F^{\text{open}} = h + \sum_{i}^{\text{closed}} (2J_i - K_i) + \sum_{i}^{\text{open}} (J_i - K_i)$$

We have chosen these forms for $V_n(C_6H_6)_{n+1}$ with spin $S = n/2$ so that the ionization from a singly (doubly) occupied orbital corresponds to the removal of an α (β) electron, implicitly assuming that the cation states have the spin state of $S - 1/2$ ($S + 1/2$).

We defined the stabilization energy ΔE as follows,

$$\Delta E = E[M_n(C_6H_6)_m] - nE[M] - mE[C_6H_6]$$

and used this value as the index for thermodynamical stability of each cluster. In fact, this stabilization energy was estimated with the RHF/ROHF, RMP2/ROMP2 (at geometry obtained by the RHF/ROHF methods), and RB3LYP/UB3LYP methods. As for the calculations of the atomic ground state energies E[M], based on the argument of Hay et al.,[13] the ROHF wavefunctions of ^{3}F(Ti), ^{4}F(V), and ^{7}S(Cr) were approximated by the single determinant of $(4s)^2(d_{z^2})^1(d_{x^2-y^2})^1$, $(4s)^2(d_{xy})^1(d_{xz})^1(d_{yz})^1$, and $(4s)^1(3d)^5$, respectively.

Extended Hückel molecular orbital (EHMO) calculations were also performed using the FORTICON8 program.[14] All the ab initio calculations were performed using the GAMESS and the Gaussian 94[15] programs with the IBM RS6000 workstations on our local network and the IBM SP2 workstation cluster of the Computer Center of the Institute for Molecular Science, Japan.

3. Results and Discussions

3.1. Orbital Interactions and Electronic Configurations of $M(C_6H_6)_2$ Complexes [M = Ti, V, and Cr]. Figure 1a shows the orbital interaction diagram of the $M(C_6H_6)_2$ complexes schematically. This diagram is drawn in view of the Aufbau principle so that the correct electronic configuration of the ground states can be predicted with the orbital ordering shown here. This type of diagram is oftenly similar to the one obtained with the EHMO calculation. As will be noted later, however, we cannot use this diagram for explaining the ionization energies.

We define as the molecular axis (z-axis) the line that passes through the metal and the centers of gravity of two benzene molecules and classify the valence orbitals in terms of their pseudoangular momenta around this axis. The five 3d orbitals of the metal atom can be divided into one dσ (d_{z^2}), two dπ (d_{xz} and d_{yz}), and two dδ (d_{xy} and $d_{x^2-y^2}$) orbitals, and of course, the 4s orbital is classified to an sσ orbital. Similarly, the six π-orbitals of benzene are one Lσ, two Lπ, two Lδ, and one Lϕ orbitals, where L means ligand. The valence electronic configurations for the isolated ground states of benzene, Ti, V, and Cr are thus $(L\sigma)^2(L\pi)^4$, $(4s)^2(3d)^2$, $(4s)^2(3d)^3$, and $(4s)^1(3d)^5$, respectively. When the two benzene molecules are located on the same position as in $M(C_6H_6)_2$, the symmetry-adapted MOs produced from them are classified into the $L(\sigma,\pi,\delta,\phi)_{g,u}$ orbitals. All the metal 3d and 4s AOs have g symmetry, and only the $L(\sigma,\pi,\delta)_g$ orbitals can interact with them. The energies of the $L(\sigma,\pi)_g$ orbitals, which are occupied in isolated benzene molecules, are lower than those of the $3d(\sigma,\pi)_g$ and $4s\sigma_g$ orbitals, and if these metal AOs were occupied, a repulsive interaction would arise. However, the dδ_g orbitals are expected to have an attractive interaction with the unoccupied Lδ_g (LUMO) orbitals. Therefore, the first four valence electrons of the metal atom are inclined to occupy the dδ_g orbitals, and the electronic configuration of $Ti(C_6H_6)_2$ is $(L\pi_g)^4(L\pi_u)^4(d\delta_g)^4$. In the cases of M = V and Cr, with five and six valence electrons, respectively, we need to find another orbital that is occupied next. Although one cannot see from only a symmetry discussion, the 4s orbital with large size has a strong repulsive interaction with the Lσ_g orbital, on the other hand, the 3dσ_g orbital does not have such an unfavorable interaction since its direction is to the "hole" in the center of benzene and it has a negligibly small interaction with the Lσ_g orbital. The dσ_g orbital then remains as the nonbonding atomic dσ_g orbital in $M(C_6H_6)_2$. Consequently, the electronic configurations of the ground states are $(L\pi_g)^4(L\pi_u)^4(d\delta_g)^4(d\sigma_g)^1$ and $(L\pi_g)^4(L\pi_u)^4(d\delta_g)^4(d\sigma_g)^2$, for M = V and Cr, respectively. In fact, it was confirmed by theoretical calculations that these configurations correspond to the ground states of the complexes. Namely, the ground states of $M(C_6H_6)_2$ with M = Ti, V, and Cr are $^1A_{1g}$, $^2A_{1g}$, and $^1A_{1g}$, respectively.[9,16−22]

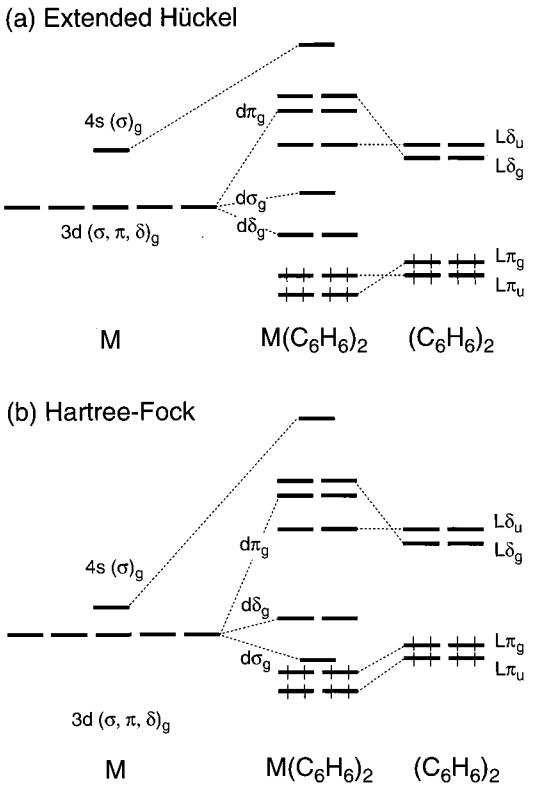

Figure 1. (a) Schematic orbital interaction diagram with the extended Hückel method for $M(C_6H_6)_2$ [M = Ti, V, and Cr]. (b) The same diagram with the Hartree−Fock method for M = V and Cr. For M = Ti, the dσ_g orbital is not occupied; therefore, it exists over the dδ_g levels. The diagrams (a) and (b) are suitable for predicting the electronic configuration of the ground states and the order of cationic states, respectively. Only ligand electrons are shown in this figure, and metal valence electronic configurations are determined by the Aufbau principle with (a). Namely, the electronic configurations for M = Ti, V, and Cr are $(\delta_g)^4$, $(\delta_g)^4(\sigma_g)^1$, and $(\delta_g)^4(\sigma_g)^2$, respectively.

3.2. Optimized Geometry and Bonding Character of $M(C_6H_6)_2$ Complexes [M = Ti, V, and Cr]. The geometries of $M(C_6H_6)_2$ [M = Ti, V, and Cr] were optimized with the RHF/ROHF, RMP2/UMP2, and RB3LYP/UB3LYP methods within the D_{6h} symmetry. The frequency analyses showed that the optimized D_{6h} structures are local minima with the DFT methods for all the complexes $M(C_6H_6)_2$ [M = Ti, V, and Cr]; however, with the other methods, there were some cases in which the D_{6h} structures were not local minima. For $Cr(C_6H_6)_2$, for example, the D_{3d} structure, in which one of the benzene

TABLE 1: Optimized Parameters of $M(C_6H_6)_2$ [M = Ti, V, and Cr] Complexes

metal	geometrical parameter	RHF/ ROHF	R/ UMP2	DFT R/ UB3LYP	previous theory	experiment
Ti	C−C	1.415	1.443	1.430	1.424[c]	
	C−H	1.072	1.089	1.084	1.068[c]	
	M−Bz[a]	1.764	1.721	1.741	1.813[c]	
	M−Bz(H)[b]	1.780	1.720	1.741		
V	C−C	1.411	1.438	1.426		
	C−H	1.072	1.088	1.084		
	M−Bz[a]	1.708	1.565	1.675		1.66[f]
	M−Bz(H)[b]	1.717	1.539	1.667		
Cr	C−C	1.405	1.432	1.420	1.417[c]	1.423[f]
					1.418[d]	
					1.436[e]	
	C−H	1.072	1.089	1.085	1.070[c]	
					1.096[d]	
	M−Bz[a]	1.675	1.592	1.621	1.723[c]	1.613[f]
					1.611[d]	
					1.614[e]	
	M−Bz(H)[b]	1.673	1.568	1.604	1.559[d]	

[a] M−Bz means the distance between the metal and the center of gravity of the benzene carbon ring. [b] M−Bz(H) means the distance between the metal and the center of gravity of the benzene hydrogen ring. [c] Reference 20. Optimized with RHF under D_{6h} symmetry. For M, the RECP of Stevens et al. with a [4121/4121/311] valence basis set is used. For C and H, the DZV bases of Dunning and Hay are used. [d] Reference 21. Optimized with DFT at the local density approximation. TZ-, DZ-, and DZ-STO basis sets are used for Cr, C, and H atoms, respectively. [e] Reference 22. Optimized with CCSD(T). The basis sets for Cr, C, and H are TZP, DZP, and DZP, respectively. [f] Reference 23.

molecules is twisted from the D_{6h} structure by 30° around *z*-axis, was a local minimum in both the RHF and RMP2 methods. However, the energy lowering from the D_{6h} structure to the D_{3d} structure was only 0.004 eV in the RHF method. For $Ti(C_6H_6)_2$, two C_1 structures were local minima and were more stable only by 0.040/0.022 eV than the D_{6h} structure. Since these energy differences were very small, we regarded the geometries of the clusters to be restricted to the D_{6h} symmetry in calculating the ionization energies.

The experimental structure parameters reported previously are 1.66, 1.613, and 1.423 Å for the V−Bz distance in $V(C_6H_6)_2$ and the Cr−Bz and C−C distances in $Cr(C_6H_6)_2$, respectively.[23] Here, the M−Bz distance means the distance between the metal and the center of gravity of the benzene carbon ring. Comparing these values in Table 1, the DFT method is found to give the most accurate values. General trends observed in Table 1 are similar to those in the previous calculations for ferrocene, in which the Hartree−Fock calculations overestimated the Fe−Cp (Cp = cyclopentadienyl) distance while the MP2 calculations underestimated it.[24] For this type of sandwich complex, importance of multireference character has been recognized.[25] Neither the Hartree−Fock nor the MP2 wavefunction takes into account this character. Although we have not known the precise reason why the DFT method works well for transition metal containing systems, these results suggest the possibility that the effect of multireference character is included in the single-determinant density functional formalism. Some previous theoretical results are also shown in Table 1. The results of RHF[20] and DFT[21] show trends similar to those of the present work, and the success of CCSD(T)[22] and the T_1 diagnosis reported there show again the importance of the multireference character.

Next, we discuss the optimized structure parameters in relation to the nature of chemical bond in these complexes. From Table 1, we can extract two trends: (1) the C−C bond lengths in the complexes are significantly longer than those in the free benzene molecule (1.384, 1.407, and 1.397 Å in RHF, RMP2, and RB3LYP, respectively), and (2) the M−Bz distance decreases as the metal changes from Ti to Cr. Although these observations were described previously,[20] we investigate their reasons in more detail and from another point of view.

TABLE 2: Bond Order Indices for the Metal−Carbon Bond of $M(C_6H_6)_2$ and Ferrocene[a]

compounds	neutral	$(\sigma_g^n)^0$	$(\pi_g^b)^0$	$(\delta_g^b)^0$
$Ti(C_6H_6)_2$	0.280		0.215 (0.065)	0.123 (0.157)
$V(C_6H_6)_2$	0.261	0.260 (0.001)	0.205 (0.056)	0.103 (0.158)
$Cr(C_6H_6)_2$	0.245	0.249 (−0.004)	0.200 (0.045)	0.090 (0.155)
ferrocene	0.170	0.231 (−0.061)	0.092 (0.078)	0.158 (0.012)

[a] The values given in parentheses denote the differences between neutral and the corresponding virtual cationic states so that they represent each MO contribution to the bond order indices.

There are two possible mechanisms for explaining the first trend. The one is the $L\pi_g \rightarrow d\pi_g$ donation and the other is the $d\delta_g \rightarrow L\delta_g$ back-donation, and both are expected to lead to the longer C−C bond distances since $L\pi$ and $L\delta$ orbitals are the HOMO and LUMO of benzene with the bonding and antibonding characters for the C−C bond, respectively. With semiempirical calculations for various first-row transition metals, Clack et al. have shown[18] that the dominant bonding interaction in MCp_2 is $L\pi \rightarrow d\pi$ donation, while that in MBz_2 is $d\delta_g \rightarrow L\delta_g$ back-donation. It is therefore worth comparing the bonding scheme in these complexes with ab initio methods. We examined the bonding character using Mayer's bond order index[26] built in the GAMESS program. This index is an extended one of Wiberg's bond order index[27] for nonorthogonal basis calculations and, as pointed out by Okada et al., it gives spin pair densities and thus gives indices for covalent bonds.[28] Mayer's indices obtained with the RHF/ROHF methods for $M(C_6H_6)_2$ and ferrocene are compiled in Table 2. Here, we emphasize that this bond order index is a nonadditive quantity with respect to the occupied orbitals. We therefore examined the contribution of each occupied orbital to the index by additionally calculating the ones for cation states without electrons in each MO to be examined, which are denoted with $(\sigma_g^n)^0$, $(\pi_g^b)^0$, and $(\delta_g^b)^0$, and subtracting them from the neutral one. Here, it should be noted that each of the σ_g^n, π_g^b, and δ_g^b orbitals is MO obtained with the RHF/ROHF method and, while σ_g^n is essentially the localized metal $d\sigma_g$ atomic orbital, π_g^b consists of benzene $L\pi_g$ with a small mixing of the metal $d\pi_g$ orbital, thus representing the $L\pi_g \rightarrow d\pi_g$ donation, and δ_g^b consists of metal $d\delta_g$ with a small component of benzene $L\delta_g$, responsible for the $d\delta_g \rightarrow L\delta_g$ back-donation.

For the V−C bond, for example, the bond order index of 0.261 is reduced to 0.205 in the configuration of $(\pi_g^b)^0$. This reduction of 0.056 is considered as the bonding contribution of the π_g^b orbitals, and that of δ_g^b is 0.158 (=0.261−0.103). From this argument, we can find that among the σ_g^n, π_g^b, and δ_g^b orbitals the δ_g^b orbitals contribute most to the bond order of the V−C bonds, and the σ_g^n orbital does little. Therefore, the lengthening of the C−C distances can be attributed not to the $L\pi_g \rightarrow d\pi_g$ donation but to the $d\delta_g \rightarrow L\delta_g$ back-donation. As shown in the remainder of Table 2, this trend is common to all three kinds of metals. On the other hand, this result is opposite to the case of ferrocene. Namely, similar to the discussion by Clack et al., the last row of Table 2 shows that the $L\pi \rightarrow d\pi$ donation is dominant and the $d\delta \rightarrow L\delta$ back-donation contributes little to the Fe−Cp bonding in ferrocene. This interesting difference can be understandable since the $L\pi$ orbital in

cyclopentadienyl has a higher energy than that in benzene and the 3d orbital of Fe has lower energy than those in Ti, V, and Cr.

The second trend mentioned above is derived from the difference in the size of d atomic orbitals, and not from the difference in the bond strength. This is explained as follows. The upper part of Table 3 shows the experimental and calculated stabilization energies for $M(C_6H_6)_2$ [M = Ti, V, and Cr]. The experimental values shown here were calculated from the heats of formation reported previously[29] with the following formula at 0 K,

$$\Delta E[M(C_6H_6)_2] = \Delta_f H[M(C_6H_6)_2, g] - 2\Delta_f H[C_6H_6, g] - \Delta_f H[M, g]$$

Although neither the theoretical methods nor the basis functions employed in this study are good enough to obtain the accurate binding energies, the values obtained with RMP2/ROMP2 and RB3LYP/UB3LYP are in better agreement with the experimental values than those with RHF/ROHF. This is because RHF/ROHF tends to overstabilize higher spin states over lower spin ones, and the spins of the ground states of these atoms and the complexes are higher and lower, respectively. Since the experimental values shown in Table 3 are dispersed largely, we cannot compare them with the calculated ones more minutely. However, at least, the M−Bz distance does not correlate to the bond strength within the framework of the MP2 or DFT methods. On the other hand, the size of the 3d atomic orbitals is known to decrease monotonously as the atomic number increases,[30] and we can relate the second trend mentioned above to the difference in the 3d atomic orbital sizes on each metal atom.[20]

On the whole, the chemical bond between the metals and benzene is mainly derived from the delocalization of the metal dδ electrons via the benzene LUMO and then is a dative bond, and this bonding character is independent of the three metals studied here. These complexes have several electronvolts of stabilization energies and are stable thermodynamically. These results explain the observation of these complexes in the mass spectra.[9]

Although, strictly speaking, we need to distinguish the δ MOs from the dδ AOs due to their significant delocalization, in the rest of paper, we shall call the former as the dδ orbitals for simplicity. The same rule applies to the dσ and dπ orbitals.

3.3. Ionization Energies of $M(C_6H_6)_2$ [M = Ti, V, and Cr] Complexes. As was noted before, an intuitive orbital diagram similar to the one obtained with the EHMO method is not suitable to describe the ionization energies. Figure 1b shows the actual orbital energy diagram obtained with the Hartree−Fock method. In the Hartree−Fock method, an orbital energy corresponds to the eigenvalue of the Fock operator, which contains an effective potential an electron in its orbital feels, and the total energy depends on the electronic configuration itself. The key point is that the total energy is not just the sum of the orbital energies. Therefore, from a view of lowering the total energy, the orbitals with lower orbital energies need not necessarily be occupied with the maximum occupation number, as the Aufbau principle states. Although these two kinds of orbital energy diagrams accord often with each other for most organic molecules, it does not hold so for transition metal containing systems in general, and we need to pay special attention to all such cases. For example, most 3d transition metal atoms have $3d^n4s^2$ configuration rather than $3d^{n+2}$ configuration, despite the orbital energy of 4s being higher than that of 3d.

TABLE 3: Stabilization Energies (eV) of $M(C_6H_6)_2$ and $M_2(C_6H_6)_3$ Complexes

species	Hartree−Fock	R/ROMP2	R/UB3LYP	experiment
$Ti(C_6H_6)_2$	1.64	−3.89	−3.63	
$V(C_6H_6)_2$	2.00	−4.05	−4.10	−4.18[b]
				−6.28[c]
$Cr(C_6H_6)_2$	3.66	−3.76	−4.13	−2.87[b]
				−3.43[d]
$Ti_2(C_6H_6)_3$	4.01	−6.55[a]	−6.58	
$V_2(C_6H_6)_3$	4.76	−7.45[a]	−7.45	
$Cr_2(C_6H_6)_3$	7.98	−5.87[a]	−7.51	

[a] MP2 energy calculated at the optimized geometry with the RHF/ROHF method. [b] These values were obtained with the collision-induced dissociation experiment for $M(C_6H_6)^+$ and $M(C_6H_6)_2^+$ in the gas phase. They were extracted from raw data under the assumption that the dissociation channel has a loose transition state. It should be noted that these values vary by an order of 1 eV with other models.[29a] [c] This value was obtained with the conventional bomb calorimetry[29b] and should be accepted with a caution for problems such as incomplete combustion of the metal and the ill-defined nature of products in this method. [d] This value was obtained from the heat of reaction with iodine vapor.[29c] This is considered to be the best one of the condensed phase data.

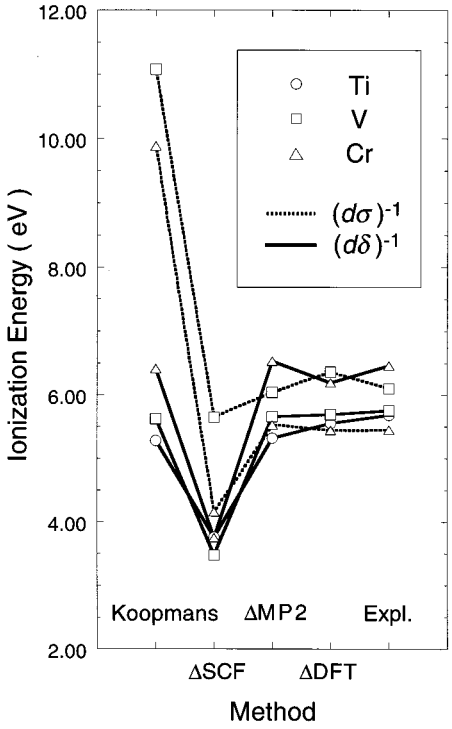

Figure 2. Ionization energies for $M(C_6H_6)_2$ [M = Ti, V, and Cr]. The symbols of circle, box, and triangle denote M = Ti, V, and Cr, respectively. The solid and dotted lines correspond to the $(d\delta_g)^{-1}$ and $(d\sigma_g)^{-1}$ ionizations, respectively.

This is because the self-energy of the 3d orbital is much larger than that of the 4s orbital since the 3d orbital is more compact than the 4s orbital.

To assess how Koopmans' theorem, ΔSCF, ΔMP2, and ΔB3LYP work well for the ionization energies, the theoretical vertical values are compared with the experimental ones in Figure 2. We should notice that, in the case of the $(\delta_g)^{-1}$ ionization for M = Ti, we adopt as the experimental value the adiabatic one (5.71 eV) obtained with the photoionization efficiency curve[9] because the vertical one reported by Cloke et al.[19] is vague (5.5−6.0 eV). All the remaining experimental values are vertical ones obtained with the photoelectron spectrum[19] and the Rydberg transitions in the gas phase

absorption spectrum.[31] Moreover, the lowest $(d\delta_g)^{-1}$ ionization of $V(C_6H_6)_2$ has been found to give a triplet state with the $(d\delta_g)^3$-$(d\sigma_g)^1$ configuration,[19] and thus the use of the Fock operators defined in section 2 is reasonable in applying Koopmans' theorem.

As a gereral trend, Koopmans' theorem was found to give reasonably accurate values for the $(\delta_g)^{-1}$ ionized states but not for the $(\sigma_g)^{-1}$ ionized states. This observation is understood in the standard way,[32] namely Koopmans' theorem often works well because the effects of orbital relaxation and electron correlation cancel each other. While this tendency is observed for the $(\delta_g)^{-1}$ ionizations, for compact molecular orbitals such as the σ_g orbital, the relaxation effect is too large to be canceled by the electron correlation effect. How about the ΔSCF? As was seen in the early study[16] comparing the photoelectron spectroscopic data with the ΔSCF calculation for $Cr(C_6H_6)_2$, ΔSCF does not necessarily give a correct order of the $(\delta_g)^{-1}$ and $(\sigma_g)^{-1}$ ionized states. To obtain the correct order, we need to include electron correlations, and ΔMP2 and ΔB3LYP predict actually the correct order, as in Figure 2.

3.4. Orbital Interactions and Electronic Configurations of Multiple-Decker Sandwich Clusters. Before discussing the actual orbital interaction, as the first approximation, we shall consider only the nearest-neighbor orbital interaction with the localized MO picture. Then, the environment around each metal atom in these complexes seems to be the same as in $M(C_6H_6)_2$; namely, each metal atom is affected only by the neighboring two benzene molecules. Therefore, the splitting pattern of the metal AOs in $M_n(C_6H_6)_{n+1}$ would resemble that in $M(C_6H_6)_2$, and the AOs on each metal atom would behave as follows. While the 4sσ and dπ orbitals are destabilized, the dδ orbitals are stabilized and the dσ orbitals are not affected by the interaction with ligand orbitals in each symmetry. By thinking in this way, we can expect that the electronic configurations of the ground states of $M_n(C_6H_6)_{n+1}$ are

$$(L\pi_1)^4(L\pi_2)^4...(L\pi_{n+1})^4(d\delta_1)^4(d\delta_2)^4...(d\delta_n)^4$$

$$(L\pi_1)^4(L\pi_2)^4...(L\pi_{n+1})^4(d\delta_1)^4(d\delta_2)^4...(d\delta_n)^4(d\sigma_1, d\sigma_2, ..., d\sigma_n)^n$$

$$(L\pi_1)^4(L\pi_2)^4...(L\pi_{n+1})^4(d\delta_1)^4(d\delta_2)^4...(d\delta_n)^4(d\sigma_1)^2(d\sigma_2)^2...(d\sigma_n)^2$$

for M = Ti, V, and Cr, respectively.

Although we considered only the nearest-neighbor orbital interaction, the same results were led from the actual orbital interaction diagram obtained with the EHMO method. Moreover, the ab initio calculations also gave the same electronic configurations for the ground states of the complexes. It should be noted that for M = V, the above electronic configuration contains the open-shell orbitals and leads to several electronic states. The problem of the state ordering of the multiplets will be discussed in section 3.7.

Next, we discuss the orbital interaction in the multiple-decker sandwich clusters concretely. Figure 3 shows the orbital energies actually obtained with the EHMO method for $V_n(C_6H_6)_{n+1}$ [$n = 1-3$]. At first sight, the splitting pattern of the orbital energies seems complicated, but we can easily understand it by separating them into each irreducible representation and applying the Hückel method in each representation.

As the basis functions for constructing the Hückel Hamiltonian, we consider only the dσ, dπ/Lπ, and dδ/Lδ orbitals for σ, π, and δ symmetries, respectively, and exclude the Lσ and Lϕ orbitals. The Hückel Hamiltonians $\mathbf{H}_{n,n+1}^{\Gamma}$ (Γ denotes the symmetry) for $M_n(C_6H_6)_{n+1}$ have the following forms.

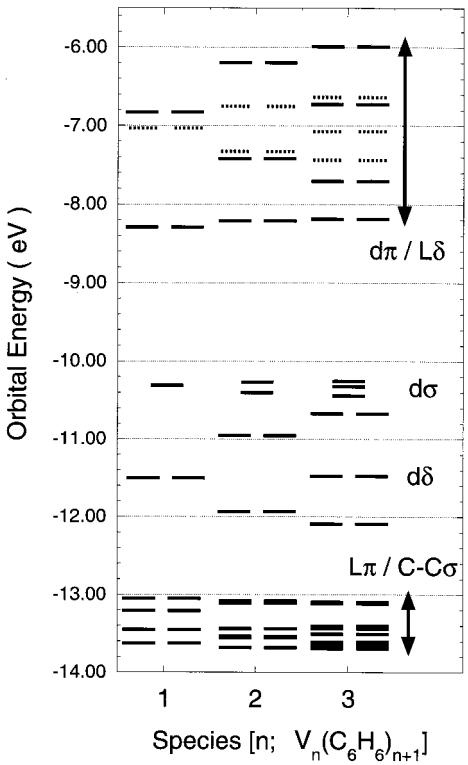

Figure 3. Molecular orbital energy levels of the mutiple-decker sandwich clusters ($V_n(C_6H_6)_{n+1}$; $n = 1-3$) obtained with the extended Hückel method. The dotted lines stand for π symmetry levels.

$$\mathbf{H}_{n,n+1}^{\sigma} = \begin{pmatrix} 0 & \beta_\sigma & & & \\ \beta_\sigma & 0 & & & \\ & & \ddots & & \\ & & & 0 & \beta_\sigma \\ & & & \beta_\sigma & 0 \end{pmatrix}$$

$$\mathbf{H}_{n,n+1}^{\pi} = \begin{pmatrix} -1 & \beta_\pi & 0 & & & & \\ \beta_\pi & 0 & \beta_\pi & & & & \\ 0 & \beta_\pi & -1 & & & & \\ & & & \ddots & & & \\ & & & & -1 & \beta_\pi & 0 \\ & & & & \beta_\pi & 0 & \beta_\pi \\ & & & & 0 & \beta_\pi & -1 \end{pmatrix}$$

$$\mathbf{H}_{n,n+1}^{\delta} = \begin{pmatrix} 1 & \beta_\delta & 0 & & & & \\ \beta_\delta & 0 & \beta_\delta & & & & \\ 0 & \beta_\delta & 1 & & & & \\ & & & \ddots & & & \\ & & & & 1 & \beta_\delta & 0 \\ & & & & \beta_\delta & 0 & \beta_\delta \\ & & & & 0 & \beta_\delta & 1 \end{pmatrix}$$

Here, in each of σ, π, and δ symmetries, the metal d orbital level was taken to be energy zero, and the energy differences dπ − Lπ and Lδ − dδ, denoted as U_Γ, were taken as the units of energy in π and δ symmetries, respectively, and the ordering of these orbitals was Lπ < d(π,δ) < Lδ. The parameters β_π and β_δ denote the resonance integrals between the dπ or dδ orbital and the neighboring benzene Lπ or Lδ orbital in each energy unit U_Γ.

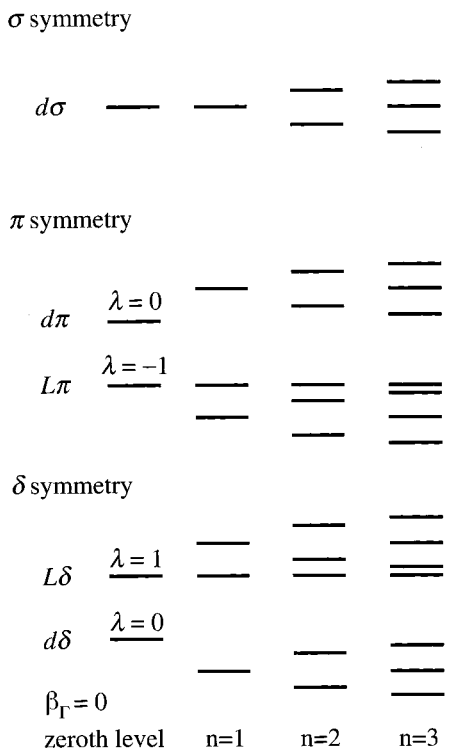

Figure 4. Same as Figure 3, but with a simple Hückel model as described in the text. Note that the distribution of the eigenvalues in δ symmetry can be obtained by an upside-down inversion of those in π symmetry with respect to $\lambda = 0$.

Moreover, the phase of these basis functions was taken so that all the resonance integrals β_Γ have the common sign, as appeared in the above Hückel Hamiltonian matrix. β_Γ has a negative value itself.

The Hückel Hamiltonian matrix for σ symmetry has the same structure as for linear chain polyenes, and the general solution is well-known as the next formula.

$$\epsilon_i = 2\beta_\sigma \cos\frac{\pi i}{n+1} \qquad (i = 1, 2, ..., n)$$

On the other hand, for π and δ symmetries, we could not succeed in obtaining the general solution, but we could find easily the recurrence relations for the secular determinants $D^{\Gamma}_{n,n+1} \equiv |\mathbf{H}^{\Gamma}_{n,n+1} - \lambda I|$ for $M_n(C_6H_6)_{n+1}$ to obtain the eigenvalues.

The matrix $\mathbf{H}^{\delta}_{n,n+1}$ can be obtained from $\mathbf{H}^{\pi}_{n,n+1}$ by changing the sign for the diagonal elements, implying that the distribution of the eigenvalues for $D^{\delta}_{n,n+1} = 0$ is simply an inverted one for $D^{\pi}_{n,n+1} = 0$ with respect to $\lambda = 0$. Another important point to be noted is, as can be verified readily, both $\mathbf{H}^{\pi}_{n,n+1}$ and $\mathbf{H}^{\delta}_{n,n+1}$ matrices have the normalized eigenvector $1/\sqrt{n+1}$ (1, 0, −1, 0, 1, ..., $(-1)^n$) with the eigenvalues of $\lambda = -1$ and $\lambda = 1$, respectively. This eigenvector acts as the HOMO within π symmetry and the LUMO within δ symmetry, as shown immediately later, and they have obviously nonbonding characters.

Figure 4 is obtained by solving the secular equations $D_{n,n+1} = 0$ for $n = 1-3$. Comparing this figure with Figure 3 by the EHMO method, it is found immediately that these orbital energy diagrams resemble each other especially for σ and δ symmetries. For π symmetry, the virtual levels behave similarly in these diagrams while the occupied levels do somewhat differently because of the non-negligible interaction among the benzene skeletal C−C bond orbitals with Lπ orbitals in the EHMO method. Therefore, the frontier orbitals, which would make energy bands for longer clusters, are found to be formed by the one-dimensional delocalization of dσ, Lπ/dπ, and Lδ/dδ orbitals.[7]

Since the magnitude of the delocalization is proportional to the resonance integrals β_Γ and therefore to the energy splitting, we can extract the degrees of the delocalization from the magnitude of the splitting in each symmetry in Figure 3 and conclude that they are largest in δ symmetry and smallest in σ symmetry. In other words, also in longer clusters, the δ orbitals contribute mostly to the bonding, and the dσ orbitals behave as nonbonding orbitals.

In this section, the simple Hückel treatment was introduced so as to understand the orbital splitting pattern in the multiple-decker sandwich clusters. In section 3.8, several properties of multiple-decker sandwich clusters will be discussed with this model.

3.5. Bonding Scheme and Thermodynamical Stability of Mutiple-Decker Sandwich Clusters. Figure 5a shows the optimized geometries with the RHF/ROHF and RB3LYP/UB3LYP methods and the bond order indices with the RHF/ROHF methods for $M_2(C_6H_6)_3$, and Figure 5b shows those with the RHF/ROHF methods for $M_3(C_6H_6)_4$. The trends of the optimized parameters are the same as for $M(C_6H_6)_2$. Namely, the M−Bz distance decreases with changing M from Ti to Cr, and the C−C distances in all these clusters are longer than that in isolated benzene. As was suggested in the last section, these results are consistent with the fact that the bonding in the multiple-decker sandwich clusters also originates mainly from the delocalization of dδ electrons via the LUMOs of benzene molecules.

The stabilization energies in the $M(C_6H_6)_2$ clusters did not depend significantly on the kinds of metal atoms. This situation also holds in $M_2(C_6H_6)_3$, as can be seen in the lower half of Table 3. Although this result may seem to contradict the fact that only $Cr_2(C_6H_6)_3$ is not observed in the mass spectra, it suggests the importance of a kinetic factor in the interpretation of the mass spectra. This aspect has been discussed previously.[9]

3.6. Reason for Large Cluster Size Dependence of Ionization Energies of Multiple-Decker Sandwich Clusters. The main purpose of the present paper is to reveal the reason why the lowest ionization energies for the multiple-decker sandwich clusters decrease drastically with increasing cluster size. In fact, we have already found the answer in the preceding discussion. Combining the δ symmetry orbital diagram in Figure 4 with Koopmans' theorem and the fact that the lowest ionization of $M(C_6H_6)_2$ (M = Ti and V) occurs from the dδ_g orbital, we may say as follows. *Increasing the size of the multiple-decker sandwich clusters leads to the formation of an electronic quasi-band structure by one-dimensional delocalization of valence electrons. The observation of the lowest ionization energies corresponds to the one from the upper end of the highest dδ band, and this band is responsible for the bonding in clusters, and then the energy change of the upper end of this band is very large with increasing cluster size.*

To confirm the above explanation, we obtained actually the ionization energies by applying Koopmans' theorem to the δ orbitals. Here, the reasonable accuracy of Koopmans' theorem for the $(\delta_g)^{-1}$ ionization of $M(C_6H_6)_2$, as was discussed in section 3.3, should be recalled. As can be seen in Figure 6, the ionization energies with Koopmans' theorem agree with the experimental ones[2,33] semiquantitatively and reproduce a significant size dependence. It should be noticed that the experi-

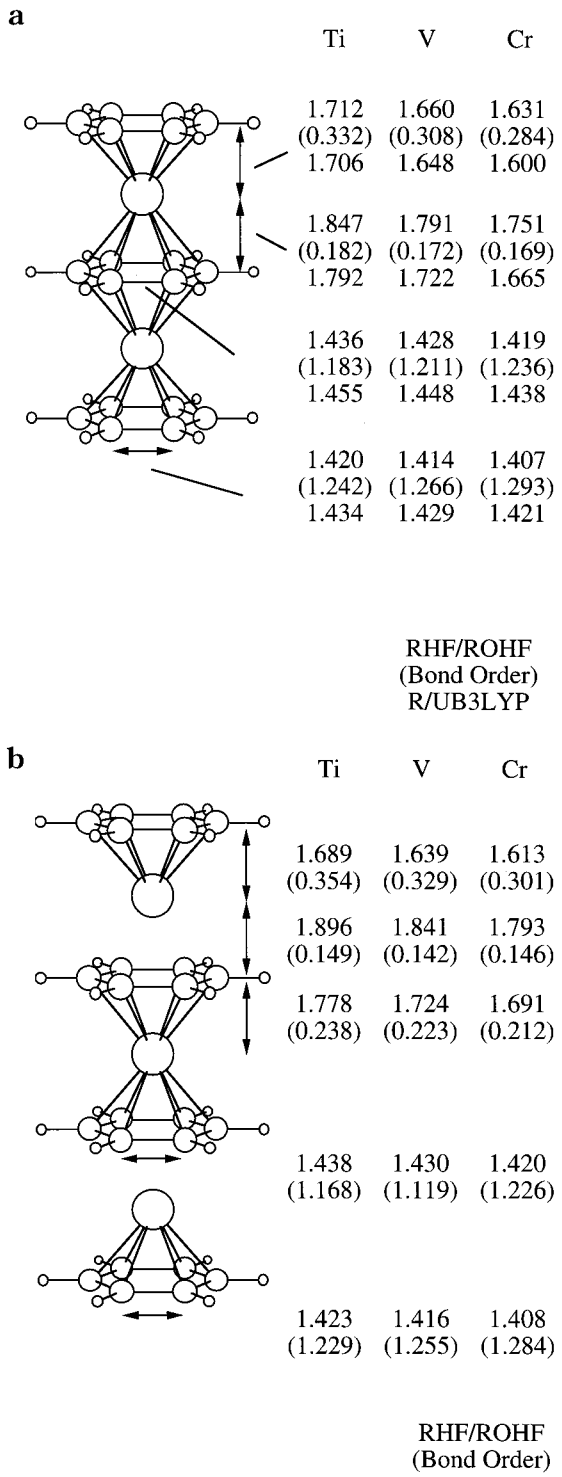

Figure 5. (a) Optimized geometries and bond order indices for $M_2(C_6H_6)_3$ [M = Ti, V, and Cr]. (b) Optimized geometries and bond order indices for $M_3(C_6H_6)_4$ [M = Ti, V, and Cr].

mental values are adiabatic ionization energies from the photoionization efficiency curves; on the other hand, the Koopmans theoretical values are, of course, vertical ones. Besides, for $Ti_3(C_6H_6)_4$, the disagreement seems to be somewhat large; however, this is within the limits of the experimental uncertainty due to the small amount of this species.[34] Judging from the above discussions, it can be considered that the above explanation for the large variation of the ionization energies of multiple-decker sandwich clusters is reasonable. Moreover, for the dδ ionization energies of $M_2(C_6H_6)_3$, the ΔMP2 gives 4.22 and 4.51 eV and ΔDFT gives 4.32 and 4.51 eV for M = Ti

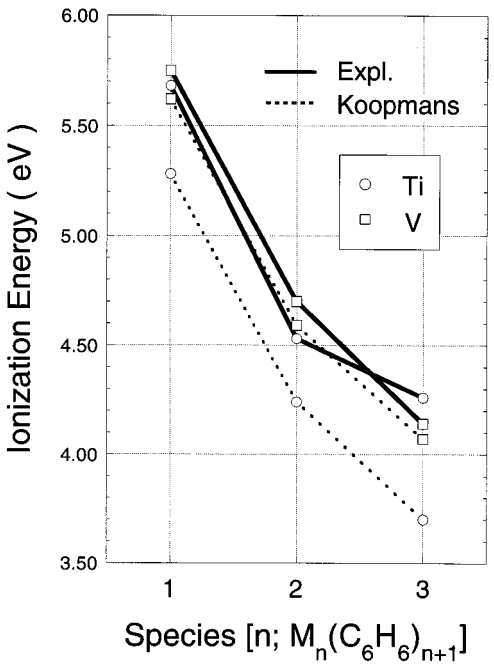

Figure 6. Experimental and calculated ionization energies for $M_n(C_6H_6)_{n+1}$ ($n = 1-3$) [M = Ti and V]. The solid and dotted lines show experimental and calculated values, respectively.

and V, respectively. These results support the usefulness of Koopmans' theorem also for "multiple-decker" species as long as the ionization is from the dδ orbitals. In these calculations, we treated $V_2(C_6H_6)_3$ and $V_3(C_6H_6)_4$ as triplet and quartet, respectively. This is because, for example, the diradical singlet and triplet states of $V_2(C_6H_6)_3$ are highly degenerate as we will see later, and while the triplet state is properly approximated within a single determinant formalism, the singlet state is not.

The fact that the large size dependence of the ionization energy could be reproduced by the one-dimensional structures can be a strong evidence for "the multiple-decker sandwich structure". So far this structure has been supported by their reactivities with molecules[2] and their ion mobilities.[35] At this stage we have succeeded in showing it also from their electronic properties. Combining all the evidence, it is concluded that $M_n(C_6H_6)_{n+1}$ has the multiple-decker sandwich structure for early transition metal M.[33]

The lowest cationic state of $Cr(C_6H_6)_2$ is $(d\sigma_g)^{-1}$ experimentally. How about the $Cr_n(C_6H_6)_{n+1}$ clusters, which have not been observed so far? We saw the failure of Koopmans' theorem for the $(d\sigma_g)^{-1}$ ionic states in section 3.3 and then needed to calculate the ionization energies with the ΔMP2 or ΔDFT methods. The values with ΔMP2 for $Cr_2(C_6H_6)_3$ were 5.49 and 6.04 eV for $(d\sigma)^{-1}$ and $(d\delta)^{-1}$, which differ from those for $Cr(C_6H_6)_2$ by -0.04 and -0.49 eV, respectively. This result agrees with our intuition in that the cluster size dependence of the ionization energies is smaller for the dσ ionization than for the dδ one because of the localized character of the dσ orbital. Extrapolating this result, we can predict the change of the lowest ionization channel, namely from dσ to dδ at $Cr_3(C_6H_6)_4$ or $Cr_4(C_6H_6)_5$. It should be noted that in the ΔMP2 calculations we used the spatial symmetry broken wavefunction for $Cr_2(C_6H_6)_3^+$; namely, we used the configuration of $(d\sigma_1)^2(d\sigma_2)^1$ instead of symmetry adapted $(d\sigma_1 + d\sigma_2)^2(d\sigma_1 - d\sigma_2)^1$, where $d\sigma_1$ and $d\sigma_2$ are essentially the atomic dσ orbitals on the two Cr atoms. While the former wavefunction is symmetry broken, it is considered to represent properly almost two noninteracting orbitals. Also for the K-shell ionizations of O_2, the symmetry

TABLE 4: Singlet−Triplet Energy Difference of $V_2(C_6H_6)_3$

method	ΔE(S−T)[a] (cm^{-1})	S^2 (singlet/triplet)[b]
UHF	4201	2.87/4.19
UMP2	−1422	
UB3LYP	46	1.06/2.07
GVB/ROHF[c]	−15	0/2
CASSCF(10/10)[d]	−11	0/2

[a] ΔE(S−T) = E(singlet) − E(triplet). If this is positive, the triplet is more stable. [b] If there is no spin contamination except for the metal dσ orbital part, the expectation value of S^2 should be unity in the singlet UHF. [c] GVB for singlet and ROHF for triplet. [d] The CAS space consists of 10 orbitals and 10 electrons.

broken wavefunction is known to yield more accurate ionization energies than the symmetry adapted one, as pointed out by Bagus and Schaefer with the ΔSCF method.[36]

3.7. Magnetic Properties of Multiple-Decker Sandwich Clusters. In section 3.4, in the case of M = V, we dared to equivocate about the state ordering of the spin multiplets of the multiple-decker sandwich clusters. This is because the molecular orbitals formed from the dσ atomic orbitals are essentially nonbonding, and we cannot determine even their ground electronic states without performing quantitative calculations. As described later, the previously emphasized charge delocalization from the dδ orbitals to the benzene LUMO can also be related to the state ordering and it actually complicates the problem, including a possibility of spin delocalization. In this section, we treat only $V_2(C_6H_6)_3$ and consider which of triplet or singlet is more stable, in other words, whether the multiple-decker sandwich cluster is ferromagnetic or diamagnetic.

Table 4 shows the singlet−triplet energy splitting for $V_2(C_6H_6)_3$ obtained with various methods. These values correspond to twice the effective exchange integral J in the Heisenberg model. In the treatment of the singlet diradical state with the spin unrestricted methods (UHF, UMP2, and UB3LYP), we made each of the two dσ orbitals localized on each metal atom with spin and spatial symmetry breakings. This treatment corresponds to optimizing an average energy (E_{av}) of the pure singlet and triplet diradical states.[32] On the other hand, we can obtain the triplet diradical energy ($E_{triplet}$) with the single determinant formalism, and therefore we have the singlet diradical energy as $2E_{av} - E_{triplet}$. Of course, more strictly for wavefunction-based methods, we should use the multiconfigurational approach such as the GVB or CASSCF method, which is free from spin contamination problems.[32] In the CASSCF calculation, we have determined the active space by inspecting the UHF natural orbitals and picking the active orbitals whose occupation numbers deviated significantly from 2 for occupied ones and from 0 for virtual ones, respectively, and made 10 orbitals (dσ_g, dσ_u, dδ_g, dδ_u, Lδ_g, Lδ_u) and 10 electrons problems.

In each of the single determinant-based methods, the energy calculation was performed on the optimized geometry for the triplet state because the singlet state is really an average state of the pure singlet and triplet states.[32] Moreover, in the cases of CASSCF and UMP2, since the geometry optimizations with these methods are very tedious, the UB3LYP and UHF triplet geometries were adopted for the single point calculations with CASSCF and UMP2, respectively. Only in the ROHF and GVB cases did we perform the geometry optimization for each pure spin state, and the result of the actual optimizations showed that the geometries of both states are essentially the same. Therefore, the use of the triplet geometry for the single point calculations of the singlet diradical can be regarded as adequate in our system. This is also justified by the final results of almost complete degeneracy between the triplet and singlet states.

The UHF result shows that the triplet state is significantly more stable than the singlet, but the UMP2 calculation gives the opposite result. As can be seen in Table 4, the values of $\langle S^2 \rangle$, the expectation value of S^2, with UHF are 2.87 and 4.19 for the singlet and triplet, respectively. The singlet and triplet UHF states, which have no spin polarization except for the metal dσ orbital part, should give 1 and 2 for $\langle S^2 \rangle$, respectively. Examining the actual spin density distribution, this remarkable spin contamination was found to originate from the large spin polarization of the dδ MOs. We observed that while in the triplet case the α spin density was large on each V atom and the β spin density was localized on the central benzene molecule, in the singlet case the spin density appeared only on the V atoms and no such spin density was on the central benzene, as can be deduced from group theory. If an intra-atomic exchange interaction within the metal d orbitals and a charge transfer interaction between the dδ MOs and the benzene LUMO are both significant, we can expect the triplet state is stabilized over the singlet state by the following mechanism. We assume first that a dσ electron on one V atom has α spin. An intra-atomic exchange interaction induces the same α spin density on the dδ orbital on this V atom. This dδ orbital has a charge transfer interaction with the benzene LUMO, which therefore tends to have opposite β spin density, which in turn induces α spin density on the dδ orbital on the other V atom. Finally, the same α spin tends to arise on the dσ orbital on the other V atom by an intra-atomic exchange interaction again. The singlet state can only be realized against the above spin delocalization mechanism. As is well-known, the UHF method overestimates the spin polarization effect in general and therefore could overstabilize the triplet state significantly in our case. Since all the remaining methods give almost the isoenergetic behavior of the singlet and triplet states and much smaller spin polarization of the dδ MOs, we should regard UHF as having overestimated the spin polarization and overstabilized the triplet state. If this is the case, convergence of the UMP series tends to be very slow and the MP2 energies are not reliable.[37] We therefore cannot help in recognizing the failure of the UHF and UMP2 methods.

It is noted that our DFT(UB3LYP) results, though based on the spin-unrestricted formalism, show little spin contamination, as in previous examples.[38−40] We also note that in the UB3LYP calculations we did not carry out spin-projection following the discussions.[40,41]

To our regret, we cannot determine confidently which state is more stable at this point; however, this degeneracy of the two spin states is very interesting in view of spin transition by means of a variation of temperature or pressure or by absorption of light.[42]

3.8. Hückel Model and Several Properties of Valence Electrons in Multiple-Decker Sandwich Clusters. In this section, using the Hückel model proposed in section 3.4, we discuss (1) the ionization energies of polymeric species $[M(C_6H_6)]_\infty$, (2) a cluster size dependence of the photoabsorption spectra, and (3) thermodynamical stability of polymeric species.

First, as seen in section 3.6, the drastic decrease of the ionization energy with increasing cluster size originates from the formation of the electronic quasi-band structure, and it was understandable also with the Hückel model. The variation of both experimental and ab initio ionization energies was so systematic that we can estimate the ones of $[M(C_6H_6)]_\infty$ denoted by IE(∞) by assuming that they behave exactly as predicted by

the Hückel model. Concretely, we solve the following two equations for β_δ and U_δ

$$\frac{(\sqrt{1+8\beta_\delta{}^2}-\sqrt{1+4\beta_\delta{}^2})}{2}U_\delta = \mathrm{IE}[\mathrm{M}(\mathrm{C_6H_6})_2] - \mathrm{IE}[\mathrm{M_2}(\mathrm{C_6H_6})_3]$$

$$\frac{(\sqrt{1+4\beta_\delta{}^2}-\sqrt{1+(8-4\sqrt{2})\beta_\delta{}^2})}{2}U_\delta = \mathrm{IE}[\mathrm{M_2}(\mathrm{C_6H_6})_3] - \mathrm{IE}[\mathrm{M_3}(\mathrm{C_6H_6})_4]$$

then we can extrapolate IE(∞) from the following equation, since the orbital energy of the HOMO converges to the atomic d orbital level, namely 0 in the limit of $n \rightarrow \infty$.

$$-\left(\frac{1-\sqrt{1+8\beta_\delta{}^2}}{2}\right)U_\delta = \mathrm{IE}[\mathrm{M}(\mathrm{C_6H_6})_2] - \mathrm{IE}(\infty)$$

Here U_δ is the energy unit for δ symmetry. The IE(∞) values for dδ ionization obtained with the above expressions were 2.68, 3.15, and 4.28 eV for M = Ti, V, and Cr, respectively. In this estimation, we used IE[$M_n(C_6H_6)_{n+1}$] by Koopmans' theorem. For M = V, we could use the experimental values, and obtained 3.00 eV as the IE(∞).

Next, we consider the photoabsorption of multiple-decker sandwich clusters. For $Cr(C_6H_6)_2$, it has been reported that the near UV absorption band at 3.87 eV (320 nm) is derived from the d$\delta \rightarrow$ Lδ transition.[17] This Lδ orbital corresponds to the orbital with $\lambda = 1$ in the Hückel treatment. We have seen that the virtual level of $\lambda = 1$ always exists independent of the cluster size and is the LUMO, as can be seen in Figure 3. (In this figure, the corresponding constant level exists around −8.2 eV and is not exactly constant because extra interactions beyond the nearest-neighbor one are also included in the EHMO method.) On the other hand, the occupied levels depend strongly on the cluster size. Figure 7 shows the actually calculated ab initio molecular orbitals that correspond to the above occupied dδ (HOMO) and the nearly constant virtual levels (LUMO). From this figure, one can see that the occupied dδ MOs always have a bonding character between the one metal atom and its neighboring benzene and that the LUMOs always have a nonbonding character between them. From these MOs, one can easily understand the size dependence of these MO energies. As a result, their size dependence of the MO energies yields the large cluster size dependence of the photoabsorption spectra in the UV−vis region.

It should be noted that the cluster size dependences of both the ionization and the photoabsorption energies originate from essentially the same origin; namely, there are both the significantly size dependent initial levels and the size independent final levels (the vacuum levels for ionization and the $\lambda = 1$ level of LUMOs for photoabsorption).

As a concrete subject, we apply the above discussion to Cr(mesitylene)$_2$ and Cr_2(mesitylene)$_3$, in which the size dependence of the band centers in the UV−vis spectra has been observed by Lamanna.[43] He has observed the bands centered at 331 and 438 nm for purified Cr(mesitylene)$_2$ and Cr_2(mesitylene)$_3$, respectively. Moreover, he has also observed the band centered at 518 nm, though he only pointed out the possibility that it might correspond to Cr_3(mesitylene)$_4$. Here, by applying the above model, we can understand the reason for the red shift with the increasing size of n and can assign the 518 nm band to Cr_3(mesitylene)$_4$ more concretely as follows. The following

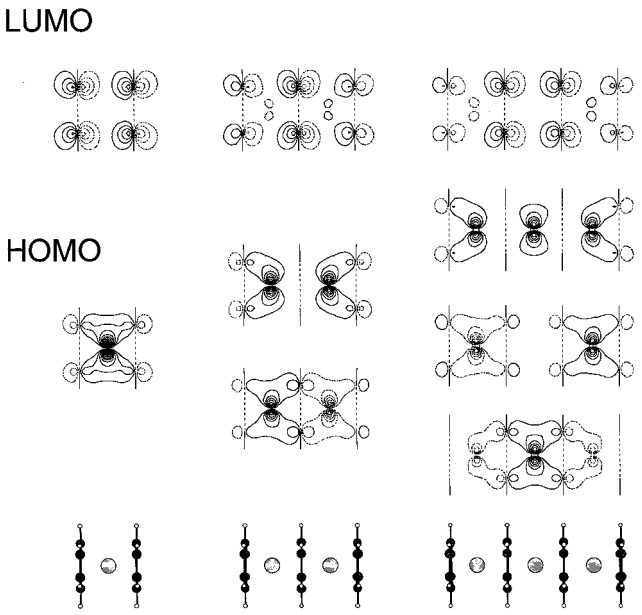

Figure 7. Contour plots of the $\delta_{x^2-y^2}$ symmetry ROHF MOs in the xz-plane containing V atoms and benzene CH groups. The z-axis is the C_6 principal rotation axis. These MOs are important for the lowest ionization and photoabsorption of $M_n(C_6H_6)_{n+1}$. The vertical direction denotes the orbital energies, and the horizontal one does the cluster size. This figure was drawn with the MacMolPlt program by Bode and Gordon.[44]

two equations are obtained for $n = 1$ and $n = 2$ by identifying their HOMO−LUMO gaps in the δ symmetry orbitals with the observed absorption bands for M(mesitylene)$_2$ and M_2(mesitylene)$_3$, respectively.

$$\frac{1+\sqrt{1+8\beta_\delta{}^2}}{2}U_\delta = 3.74\ (\mathrm{eV})$$

$$\frac{1+\sqrt{1+4\beta_\delta{}^2}}{2}U_\delta = 2.83\ (\mathrm{eV})$$

By solving these equations for β_δ and U_δ and substituting these values for the following expression of the HOMO−LUMO gap for $n = 3$,

$$\frac{1+\sqrt{1+(8-4\sqrt{2})\beta_\delta{}^2}}{2}U_\delta$$

we obtained 2.32 eV (533 nm) for Cr_3(mesitylene)$_4$. Therefore, as noted above, we can conclude confidently that the 518 nm peak is due to Cr_3(mesitylene)$_4$.

We note that the HOMOs always have g symmetry and the LUMOs u symmetry and the HOMO−LUMO excitation is essentially a metal to benzene charge transfer excitation and should be strongly allowed independent of the cluster size.

Finally, we discuss the thermodynamical stability of polymeric species $[M(C_6H_6)]_\infty$. From Figure 4, one can expect that the stabilization energies of $M_n(C_6H_6)_{n+1}$ defined in section 2 are approximately proportional to n, and the stabilization energies per MC_6H_6 unit are constant with respect to n. As a simple example, we shall concentrate on the stabilization energies by electrons in the δ symmetry orbitals for $n = 1-3$. The lowest part of Figure 4 shows that for both $n = 2$ and 3, the average energies of the occupied levels are almost the same as that of the occupied level for $n = 1$. This means that the stabilization energies are proportional to n.

Strictly speaking, this statement is not correct, but the deviation from such behavior was very small, and thus one can regard that the stabilization energy per MC_6H_6 unit is nearly constant for any n of $M_n(C_6H_6)_{n+1}$. Namely, this predicts the thermodynamical stability of $M_n(C_6H_6)_{n+1}$ with $n = \infty$, and thus the upper limit[34] of $n = 7$ for experimentally observed multiple-decker sandwich clusters (M = V) must be governed by a kinetic factor in the formation process of the clusters.

4. Conclusion

All the above discussion made it clear that both the bonding and the large dependence of ionization energies with the cluster size are derived from the delocalization of the dδ electrons on metal atoms via the LUMOs of benzene. In particular, we could successfully reproduce the cluster size dependence of the ionization energies. This can be strong theoretical evidence for the observed clusters $M_n(C_6H_6)_{n+1}$ to have multiple-decker sandwich structures for early transition metals M.[33] Moreover, the suggested Hückel model predicts no deterioration of the stabilization energies with increasing cluster size, and at least, much longer clusters can be considered to be thermodynamically stable. The formation of longer clusters or even one-dimensional bulky material may be possible.

Acknowledgment. This study is the result of daily cooperation with Prof. K. Kaya and Prof. A. Nakajima. We would like to thank them. We gratefully acknowledge helpful discussions with Dr. T. Kurikawa on experimental results of the multiple-decker sandwich clusters. We also thank the Computer Center of the Institute for Molecular Science for the use of computers. This work was supported in part by a Grants-in-Aid for Scientific Research from the Minister of Education, Science, Culture, and Sports of Japan.

References and Notes

(1) For example: Freiser, B. S., Ed. *Organometallic Ion Chemistry*; Kluwer Academic Publishers: Dordrecht, Netherlands, 1995.

(2) Hoshino, K.; Kurikawa, T.; Takeda, H.; Nakajima, A.; Kaya, K. *J. Phys. Chem.* **1995**, *99*, 3053.

(3) (a) Kurikawa, T.; Hirano, M.; Takeda, H.; Yagi, K.; Hoshino, K.; Nakajima, A.; Kaya, K. *J. Phys. Chem.* **1995**, *99*, 16428. (b) Nagao, S.; Kurikawa, T.; Miyajima, K.; Nakajima, A.; Kaya, K. *J. Phys. Chem. A* **1998**, *102*, 4495.

(4) Buchanan, J. W.; Reddic, J. E.; Grieves, G. A.; Duncan, M. A. *J. Phys. Chem A* **1998**, *102*, 6390.

(5) Guo, B. C.; Kerns, K. P.; Castleman, A. W., Jr. *Science* **1992**, *255*, 1411.

(6) Thorne, R. E. *Physics Today* **1996**, *5*, 42.

(7) Burdett, J. K.; Canadell, E. *Organometallics* **1985**, *4*, 805.

(8) (a) Kuhlmann, T.; Roth, S.; Roziere, J.; Siebert, W. *Angew. Chem.* **1986**, *98*, 87. (b) Lavrentiev, M. Y.; Köppel, H.; Böhm, M. C. *Chem. Phys.* **1993**, *169*, 85.

(9) Yasuike, T.; Yabushita, S.; Nakajima, A.; Kaya, K. *J. Phys. Chem. A* **1997**, *101*, 5360.

(10) Huzinaga, S.; Andzelm, J.; Klobukowski, M.; Radzio-Andzelm, E.; Sakai, Y.; Tatewaki, H. *Gaussian Basis Sets for Molecular Calculations*; Elsevier: Amsterdam, 1984.

(11) Schmidt, M. W.; Baldridge, K. K.; Boatz, J. A.; Elbert, S. T.; Gordon, M. S.; Jensen, J. H.; Koseki, S.; Matsunaga, N.; Nguyen, K. A.; Su, S. J.; Windus, T. L.; Dupuis, M.; Montgomery, J. A. GAMESS. *J. Comput. Chem.* **1993**, *12*, 1347.

(12) (a) Becke, A. D. *J. Chem. Phys.* **1993**, *98*, 5648. (b) Lee, C.; Yang, W.; Parr, R. G. *Phys. Rev. B* **1988**, *37*, 785.

(13) Hay, P. J. *J. Chem. Phys.* **1977**, *66*, 4377.

(14) Howell, J.; Rossi, A.; Wallace, D.; Haraki, K.; Hoffmann, R. FORTICON8. QCPE Program No. 517.

(15) Frisch, M. J.; Trucks, G. W.; Schlegel, H. B.; Gill, P. M. W.; Johnson, B. G.; Robb, M. A.; Cheeseman, J. R.; Keith, T. A.; Petersson, G. A.; Montgomery, J. A.; Raghavachari, K.; Al-Laham, M. A.; Zakrzewski, V. G.; Ortiz, J. V.; Foresman, J. B.; Cioslowski, J.; Stefanov, B. B.; Nanayakkara, A.; Challacombe, M.; Peng, C. Y.; Ayala, P. Y.; Chen, W.; Wong, M. W.; Andres, J. L.; Replogle, E. S.; Gomperts, R.; Martin, R. L.; Fox, D. J.; Binkley, J. S.; Defrees, D. J.; Baker, J.; Stewart, J. P.; Head-Gordon, M.; Gonzalez, C.; Pople, J. A. Gaussian 94 (Revision D.2); Gaussian, Inc.: Pittsburgh, PA, 1995.

(16) Guest, M. F.; Hillier, I. H.; Higginson, B. R.; Lloyd, D. R. *Mol. Phys.* **1975**, *29*, 113.

(17) Weber, J.; Geoffroy, M.; Goursot, A.; Pénigault, E. *J. Am. Chem. Soc.* **1978**, *100*, 3995.

(18) Clack, D. W.; Warren, K. D. *Struct. Bonding* **1980**, *39*, 1.

(19) Cloke, F. G. N.; Dix, A. N.; Green, J. C.; Perutz, R. N.; Seddon, E. A. *Organometallics* **1983**, *2*, 1150.

(20) King, W. A.; Bella, S. D.; Lanza, G.; Khan, K.; Duncalf, D. J.; Cloke, F. G. N.; Fragala, I. L.; Marks, T. J. *J. Am. Chem. Soc.* **1996**, *118*, 627.

(21) Bérces, A.; Ziegler, T. *J. Phys. Chem.* **1994**, *98*, 13233.

(22) Lüthi, H. P. *J. Mol. Struct.* **1996**, *388*, 299.

(23) Muetterties, E. L.; Bleeke, J. R.; Wucherer, E. J.; Albright, T. A. *Chem. Rev.* **1982**, *82*, 499.

(24) (a) Lüthi, H. P.; Ammeter, J. H.; Almöf, J.; Faegri, K., Jr. *J. Chem. Phys.* **1982**, *77*, 2002. (b) Park, C.; Almlöf, J *J. Chem. Phys.* **1991**, *95*, 1829.

(25) (a) Lüthi, H. P.; Siegbahn, P. E. M.; Almlöf, J.; Faegri, K., Jr.; Heiberg, A. *Chem. Phys. Lett.* **1984**, *111*, 1. (b) Pierloot, K.; Persson, B. J.; Roos, B. O. *J. Phys. Chem.* **1995**, *99*, 3465.

(26) (a) Mayer, I. *Int. J. Quantum. Chem.* **1986**, *29*, 73. (b) Villar, H. O.; Dupuis, M. *Chem. Phys. Lett.* **1987**, *142*, 59.

(27) Wiberg, K. A. *Tetrahedron* **1968**, *24*, 1083.

(28) Okada, T.; Fueno, T. *Bull. Chem. Soc. Jpn.* **1975**, *48*, 2025.

(29) (a) Meyer, F.; Khan, F. A.; Armentrout, P. B. *J. Am. Chem. Soc.* **1995**, *117*, 9740. (b) Fischer, E. O.; Reckziegel, A. *Chem. Ber.* **1961**, *94*, 2204. (c) Connor, J. A.; Skinner, H. A.; Virmani, Y. *J. Chem. Soc., Dalton Trans. 1* **1972**, *68*, 1754.

(30) Emsley, J. *The Elements*, 2nd ed.; Clarendon: Oxford, U.K., 1991.

(31) Ketkov, S. Y.; Domrachev, G. A.; Razuvaev, G. A. *J. Mol. Struct.* **1989**, *195*, 175.

(32) Szabo, A.; Ostlund, N. S. *Modern Quantum Chemistry: Introduction to Advanced Electronic Structure Theory*; Dover Publications: New York, 1996.

(33) Kurikawa, T.; Takeda, H.; Hirano, M.; Judai, K.; Arita, T.; Nagao, S.; Nakajima, A.; Kaya, K. *Organometallics* **1999**, *18*, 1430.

(34) Kurikawa, T.; Nakajima, A.; Kaya, K. Private communication.

(35) Weis, P.; Kemper, P. R.; Bowers, M. T. *J. Phys. Chem. A* **1997**, *101*, 8207.

(36) Bagus, P. S.; Schaefer, H. F., III. *J. Chem. Phys.* **1972**, *56*, 224.

(37) Handy, N. C.; Knowles, P. J.; Somasundram, K. *Theor. Chim. Acta* **1985**, *68*, 87.

(38) Lee, A. M.; Handy, N. C. *J. Chem. Soc., Faraday Trans.* **1993**, *89*, 3999.

(39) Baker, J.; Muir, M.; Andzelm, J. *J. Chem. Phys.* **1995**, *102*, 2063.

(40) Pople, J. A.; Gill, P. M. W.; Handy, N. C. *Int. J. Quantum Chem.* **1995**, *56*, 303.

(41) Cremer, D.; Kraka, E.; Szalay, P. G. *Chem. Phys. Lett.* **1998**, *292*, 97.

(42) For example: Kahn, O. *Molecular Magnetism*; VCH: New York, 1993.

(43) Lamanna, W. M. *J. Am. Chem. Soc.* **1986**, *108*, 2096.

(44) Bode, B. M.; Gordon, M. S. *J. Mol. Graphics Modeling*, in press.